Continuous and comprehensive atmospheric observations in Beijing : a station to understand the complex urban atmospheric environment

Liu, Yongchun

2020

Continuous and comprehensive atmospheric observations in Beijing: a station to understand the complex urban atmospheric environment

Yongchun Liu, Chao Yan, Zemin Feng, Feixue Zheng, Xiaolong Fan, Yusheng Zhang, Chang Li, Ying Zhou, Zhuohui Lin, Yishou Guo, Ying Zhang, Li Ma, Wenshuo Zhou, Zhikun Liu, Lubna Dada, Kaspar Dällenbach, Jenni Kontkanen, Runlong Cai, Tommy Chan, Biwu Chu, Wei Du, Lei Yao, Yonghong Wang, Jing Cai, Juha Kangasluoma, Tom Kokkonen, Joni Kujansuu, Anton Rusanen, Chenjuan Deng, Yueyun Fu, Rujing Yin, Xiaoxiao Li, Yiqun Lu, Yiliang Liu, Chaofan Lian, Dongsen Yang, Weigang Wang, Maofa Ge, Yuesi Wang, Douglas R. Worsnop, Heikki Junninen, Hong He, Veli-Matti Kerminen, Jun Zheng, Lin Wang, Jingkun Jiang, Tuukka Petäjä, Federico Bianchi & Markku Kulmala

View supplementary material

Published online: 13 Oct 2020.

Submit your article to this journal

🔓 OPEN ACCESS | Check for updates |

Continuous and comprehensive atmospheric observations in Beijing: a station to understand the complex urban atmospheric environment

Yongchun Liu [ID][a], Chao Yan[a,b], Zemin Feng[a], Feixue Zheng[a], Xiaolong Fan[a], Yusheng Zhang[a], Chang Li[a], Ying Zhou[a], Zhuohui Lin[a], Yishou Guo[a], Ying Zhang[a], Li Ma[a], Wenshuo Zhou[a], Zhikun Liu[a], Lubna Dada[b], Kaspar Dällenbach[b], Jenni Kontkanen[b], Runlong Cai[b,c], Tommy Chan[b], Biwu Chu[b,d], Wei Du[b], Lei Yao[b], Yonghong Wang[b], Jing Cai[b], Juha Kangasluoma[a,b], Tom Kokkonen[b], Joni Kujansuu[a,b], Anton Rusanen[b], Chenjuan Deng[c], Yueyun Fu[c], Rujing Yin[c], Xiaoxiao Li[c], Yiqun Lu[e], Yiliang Liu[e], Chaofan Lian[f], Dongsen Yang[g], Weigang Wang[f], Maofa Ge[f], Yuesi Wang[h], Douglas R. Worsnop [ID][i], Heikki Junninen[j], Hong He[d], Veli-Matti Kerminen[b], Jun Zheng[g], Lin Wang[e], Jingkun Jiang[c], Tuukka Petäjä [ID][a,b,k], Federico Bianchi[b] and Markku Kulmala [ID][a,b,k]

[a]Aerosol and Haze Laboratory, Beijing Advanced Innovation Center for Soft Matter Science and Engineering, Beijing University of Chemical Technology, Beijing, China; [b]Institute for Atmospheric and Earth System Research/Physics, Faculty of Science, University of Helsinki, Helsinki, Finland; [c]State Key Joint Laboratory of Environment Simulation and Pollution Control, State Environmental Protection Key Laboratory of Sources and Control of Air Pollution Complex, School of Environment, Tsinghua University, Beijing, China; [d]State Key Joint Laboratory of Environment Simulation and Pollution Control, Research Center for Eco-Environmental Sciences, Chinese Academy of Sciences, Beijing, China; [e]Department of Environmental Science & Engineering, Fudan University, Shanghai, China; [f]State Key Laboratory for Structural Chemistry of Unstable and Stable Species, Beijing National Laboratory for Molecular Sciences, Institute of Chemistry, Chinese Academy of Sciences, Beijing, China; [g]Jiangsu Key Laboratory of Atmospheric Environment Monitoring and Pollution Control, Nanjing University of Information Science & Technology, Nanjing, China; [h]State Key Laboratory of Atmospheric Boundary Layer Physics and Atmospheric Chemistry, Institute of Atmospheric Physics, Chinese Academy of Sciences, Beijing, China; [i]Aerodyne Research Inc., Billerica, Massachusetts, USA; [j]Institute of Physics, University of Tartu, Tartu, Estonia; [k]Joint International Research Laboratory of Atmospheric and Earth System Sciences, School of Atmospheric Sciences, Nanjing University, Nanjing, China

ABSTRACT

Due to profound impact on climate and human health, air quality has attracted attention from all levels of the civil society. The key step in the provision of required tools for the society to tackle the complex air quality problem is to characterize it in a comprehensive manner with a long-term perspective. Here, we describe a continuous and comprehensive observation station and its accompanying state-of-the-art instrumentation that was established to investigate the complex urban atmospheric environment in a rapidly developing Chinese Megacity. The station, located in downtown Beijing, aims to study air

---

CONTACT Yongchun Liu ✉ liuyc@buct.edu.cn 🖂 Aerosol and Haze Laboratory, Beijing University of Chemical Technology, China; Federico Bianchi ✉ federico.bianchi@helsinki.fi 🖂 Institute for Atmospheric and Earth System Research/Physics, Faculty of Science, University of Helsinki, Helsinki, Finland; Markku Kulmala ✉ markku.kulmala@helsinki.fi 🖂 Institute for Atmospheric and Earth System Research/Physics, Faculty of Science, University of Helsinki, Helsinki, Finland
🔵 Supplemental data for this article can be accessed here.

quality by identifying the major atmospheric pollutants and key processes determining their formation and loss mechanisms. A few hundreds of parameters are continuously measured with the state-of-the-art instruments, including trace gas concentrations, aerosol particle size distributions, and mass concentrations, covering aerosol particle chemical composition from molecules to micrometer-sized aerosol particles. This produced long-term, comprehensive big data with around 1×10^{11} bytes per year. In this paper, we provide an overview on the facilities of the station, the instrumentation used, the workflow of continuous observations and examples of results from 2018 to 2019 and a basis for establishing a modern long-term, comprehensive atmospheric urban observation station in other megacities.

1. Background: short review of air pollution in China

Air pollution has become a serious environmental issue in the world since 1950s when the London smog (dominated by H_2SO_4 and particulate matter (PM)) (Davis, Bell, & Fletcher, 2002) and Los Angeles smog (dominated by O_3, peroxyacetyl nitrate (PAN) and PM) (Hidy, 2018) became iconic events. Over the last four decades, the developed countries in Europe and North-America, and elsewhere have implemented policies to phase out or update such technologies in industries, transportation, and agriculture that contribute to severe air pollution because it threatens public health through both acute (Bell, Davis, & Fletcher, 2004) and long-term adverse effects (Lelieveld, Evans, Fnais, Giannadaki, & Pozzer, 2015). As a consequence, China has transformed into the world's factory (Zhang & Samet, 2015), accompanied with the bloom of economy and the shifting of heavy air pollution to China (Zhang et al., 2017) due to the lagging in clean production technologies.

Air pollution in China started from the acid rain problem (Larssen et al., 1999, 2006) due to the extensive use of coal since 1970s (Larssen et al., 2006), increasing from 404.0 million metric tons of standard coal equivalent (Mtce) in 1978 to 2712.0 Mtce in 2017 (http://www.stats.gov.cn). The Eastern and Southern China is one of the three major regions (together with Europe and America) of acid rain in the world. The precipitation pH in 17 of the 23 provinces (with 22.5% of the land area) was lower than 5.6 in 1990s, rising to 18 provinces (with 30.5% of the land area) in 2010s (Yu et al., 2017a). In 1980s, the Renewable Energy Law and the Cleaner Production Promotion Law were launched to control acid deposition (Yu et al., 2017a). In 1998, China approved the division scheme of sulfur dioxide pollution and acid rain control zones. Nowadays, the areas of heavy acid deposition have been reduced to some extent (Yu et al., 2017a, 2017b), but the areas of moderate acid deposition have been expanding into previously undeveloped provinces (Yu et al., 2017a). In the early stages, acid rain in China was dominated by SO_4^{2-}, while the role of NO_3^- has increased gradually (Sun et al., 2018; Wen et al., 2018).

In 1979, photochemical smog pollution indicated by high concentration of O_3 (with maximum hourly mean O_3 concentration varied from 80 to 122 ppbv on polluted days in July), PAN and PM was for the first time observed at Xigu district in Lanzhou (Tian et al., 1980), followed by the first study of photochemical smog pollution in China in 1980s (Tang, Li, & Dong, 1989). Then, emissions of NO_x and volatile organic compounds (VOCs) increased prominently because the industries grew vigorously in 1990s and the

population of private vehicles increased significantly (Wang, Teter, & Sperling, 2011). This resulted in summertime photochemical smog pollution (Hallquist et al., 2016) and a mixture of London-type smog and photochemical smog in many regions in China (Zhang and Samet, 2015). As an indicator of photochemical smog, O_3 concentration in Beijing have increased sharply since the 1990s, and often exceed 200 ppbv (Shao, Tang, Zhang, & Li, 2006). In September 2001, high concentrations (>120 ppbv) of O_3 were observed at a rural coastal site in western Hong Kong for six consecutive days, with maximum 1-h O_3 concentration reaching 191 ppbv (Wang & Kwok, 2003). Since 2005, the number of photochemical smog studies has increased drastically in China, especially in Pearl River Delta (PRD), Beijing-Tianjin-Hebei (BTH), and Yangtze River Delta (YRD) (Wang et al., 2017a). Atmospheric O_3 concentrations in urban Beijing demonstrated a significant upward-trend at both seasonal and inter-annual scales (from 30 to 37 ppbv) during 2006–2016 (Chen et al., 2019b) with an increased rate of 1.1% yr^{-1} (Chen et al., 2019b; Tang, Li, Wang, Xin, & Ren, 2009). In the Northern China Plain (NCP), a large increase rate (2.0% yr^{-1}) of boundary-layer ozone was observed in the summertime during 1995–2005 based on aircraft data (Wang et al., 2017a), while a rate of 0.86 ppbv yr^{-1} was observed in Guangdong from 2006 to 2011 (Li et al., 2014). Nowadays, O_3 pollution in summer is more and more prominent in China. O_3 formation is VOCs-limited in most regions of China due to high concentrations of NO_x (Ma, Xu, Zhao, & Yan, 2012; Wang et al., 2017a). This is opposite to the NO_x-limited regime in USA (Laughner & Cohen, 2019).

In past decades, haze due to very high loading of fine particles has become a widespread environmental problem in BTH, PRD, YRD, and Sichuan basin (SCB), with a low horizontal visibility (<10 km) particularly in winter. In the case of haze, relative humidity (RH) is below 90% to separate these from fog events. The frequency of haze events increased from ~40 days yr^{-1} in 1981 to >120 days yr^{-1} in 2010 in the BTH region (Fu, Xu, Yang, Li, & Zhao, 2014). In particular, after China's accession into World Trade Organization (WTO) in 2001, the economic growth in China has experienced a dramatic rise both in energy demand and in production (Zheng et al., 2020). This obviously aggravated the deterioration of air quality (Wang et al., 2014), although stringent emission standards have been enforced. During 2004–2013, the average $PM_{2.5}$ concentrations were >100 μg m^{-3} with an increased rate of 0.75 μg m^{-3} yr^{-1} in BJH, >85 μg m^{-3} in SCB and YRD and >55 μg m^{-3} in PRD (Ma et al., 2016). In January 2013, a severe haze event occurred across a total area of ~1.3 million km^2 and affected ~800 million people (An et al., 2019). The hourly $PM_{2.5}$ concentration in Beijing even exceeded 1000 μg m^{-3} (Zhang et al., 2019).

During the past few years, intensive research programs have been initiated, such as Study on the Formation Mechanism of Air Pollution and Control Technology from the National Key R&D Program of China (2015-), Formation mechanism, Health Effects and Coping Strategy of Complex Air Pollution in China from National Natural Science Foundation of China (2015-), Haze Formation Mechanism and Control Technology from the Strategic Priority Research Program of Chinese Academy of Sciences (2012–2017). Based on these research programs, remarkable progress has been achieved in understanding on the causes of haze in China. For example, local emissions (An et al., 2019), regional transport (Zheng et al., 2015), and secondary formation (He et al., 2018; Huang et al., 2014) of pollutants under favorable meteorological conditions (Liu et al., 2017; Zhu et al., 2018) have been identified as the driving forces of haze events. As for the secondary formation of aerosol, a concept of haze chemistry, whose intrinsic characteristics is the synergistic effect among different gas-phase

and/or particle-phase pollutants on secondary processes leading to increase in aerosol number (Chu et al., 2019; Kerminen et al., 2018) and mass concentrations (Cheng et al., 2016; Guo et al., 2014; Huang et al., 2014; Wang et al., 2016; Xue et al., 2019), has been proposed (Cheng et al., 2016). Such complex effects have been supported by sulfate formation via heterogeneous oxidation from SO_2 promoted by H_2O_2 and/or NO_2 on mineral dust (He et al., 2014; Huang, Zhao, Li, & Chen, 2015), catalytic oxidation of SO_2 by black carbon (Zhang et al., 2020), aqueous oxidation of SO_2 promoted by NO_2 in the presence or absence of NH_3 in particle-bound water film (He et al., 2014; Wang et al., 2016), nitrate formation via efficient hydrolysis of N_2O_5 on aerosol surfaces (Wang et al., 2017b), and haze formation induced by new particle formation (Guo et al., 2014; Zamora et al., 2019) and further growth (Guo et al., 2020). About the interaction between meteorological parameters and haze formation, a comprehensive meteorological index (PLAM), indicating regional atmospheric stability and air condensation ability has been proposed (Zhang, Zhong, Wang, Wang, & Liu, 2018). The negative feedback mechanisms between the boundary layer meteorology and haze accumulation has been proposed (Ding et al., 2016b; Petäjä et al., 2016; Wang et al., 2020) and the aggravation effect of air quality by worsening of meteorological conditions, such as decrease in the wind speed (Fu et al., 2014) and boundary-layer height (Zhong et al., 2018), has also been quantified.

In 2013, the State Council of China promulgated the toughest-ever Air Pollution Prevention and Control Action Plan (Tang et al., 2019; Zhang et al., 2019). As a consequence, the annual averaged $PM_{2.5}$ concentrations across the nation (74 cities, 536 sites) decreased significantly from 69.8 µg m^{-3} in 2013 to 47.3 µg m^{-3} in 2017 (Chen, Liu, Ban, Zhao, & Chen, 2019a; Tang et al., 2019; Zhang et al., 2019). In Beijing, it decreased from 89.5 µg m^{-3} in 2013 to 58.0 µg m^{-3} in 2017 (Cheng et al., 2019). Variations in meteorological conditions, sometimes responsible for more than 50% of changes in local air quality (Zhang et al., 2018), were estimated to explain only 9 % of the national decrease in $PM_{2.5}$ concentrations from 2013 to 2017 (Zhang et al., 2019). These results highlight the efficiency of the Action Plan.

It should be noted that acid rain is still an environmental problem and the $PM_{2.5}$ concentrations in most regions of China are still significantly higher than the air quality standard of World Health Organization. At the same time, ozone pollution has become more and more severe (Chen et al., 2019b). Therefore, many scientific questions on air pollution remain open and need to be clarified, such as the crucial factors determining the formation of key secondary pollutants, air quality impacts on human health, and complicated interactions and feedbacks between the air quality, global climate, regional meteorology, and ecosystem processes. Thus, a multidisciplinary approach by scientists from different fields need to be utilized in the future. The key step in the provision of required tools for the society to tackle the complex air quality problems is to characterize the air pollution in a comprehensive manner with a long-term perspective (Petäjä et al., 2020). The experiences from these acts on air pollution also confirmed the importance of comprehensive atmospheric observation for air pollution prevention.

At the present time, several observation networks focusing on meteorology, atmosphere, and ecosystems are running around the world, such as the Global Atmospheric Watch (GAW) since 1950s, the Long-Term Ecological Research Network (LTER) since 1980, the Chinese Ecosystem Research Network (CERN, China) since 1988 (Hu, Wang, & Liu, 2007), the Environment Change Network (ECN, UK) since 1992, the Aerosol, clouds, and

Trace gases Research InfraStructure Network (ACTRIS, Europe) since 2015, the Station for Measuring Ecosystem Atmosphere Relations (SMEAR) since 1991 (Hari et al., 2016), and Station for Observing Regional Processes of the Earth System (SORPES) in Nanjing since 2011 (Ding et al., 2016a).

An observation station is a fundamental element for these observation networks. It is very important to share the ideas and experiences on constructing a modern urban observation station in the atmospheric environment society. In this work, we will introduce a newly established continuous and comprehensive atmosphere observation station, that's, Aerosol and Haze Laboratory/Beijing University of Chemical Technology Station (AHL/BUCT Station), in a megacity Beijing. It has state-of-the-art facilities that are responding to the societal needs pertinent to air quality. One of the main aims was to produce big, ground base atmospheric data and contribute to the global observatory (Kulmala, 2018). Therefore, we developed and constructed AHL/BUCT station. The long-term goals of the AHL/BUCT Station are to identify the crucial pollutants and key processes governing air pollution in the megacities, to understand the sources of crucial air pollutants, to quantify the formation mechanism of secondary pollutants and to assess the possible impacts of air pollution on human health, climate change and ecological systems.

2. Methodology

2.1. Location of the AHL/BUCT station

Downtown Beijing area is surrounded by the Taihang mountain cordillera from the west (Xishan) and the Yanshan mountain cordillera from the north (Jundushan). This leads to a half-basin terrain as shown in Figure 1. The AHL/BUCT Station is located in the main teaching building of the west campus of Beijing University of Chemical Technology (Lat. 39°56′31″ and Lon. 116°17′52″), which is ~9.0 km away from Xishan and ~30 km from Jundushan, respectively. The building is surrounded by three roads, one located 550 m from
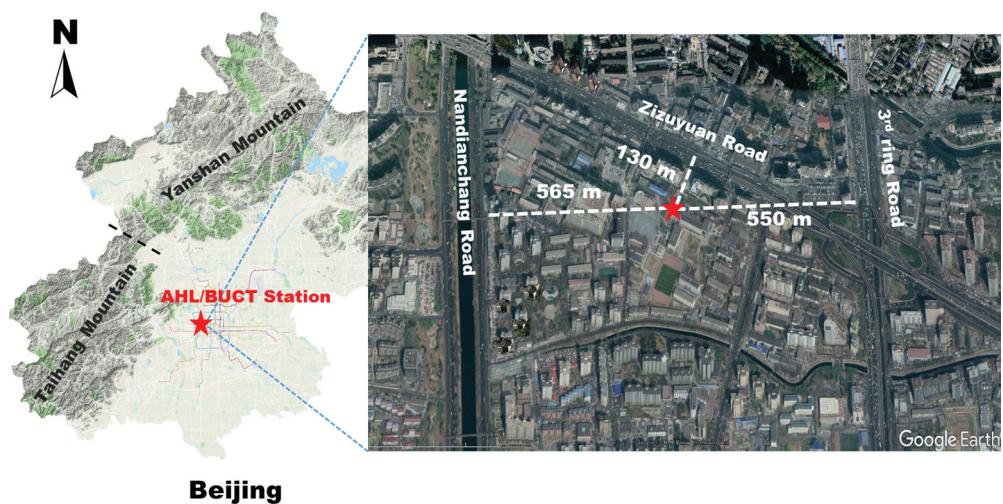
Figure 1. The location of AHL/BUCT Station.

the 3rd ring road in the East, another one 130 m from the Zizhuyuan road in the North and yet another one 565 m from the Nandianchang road in the West. Therefore, the AHL/BUCT Station is a typical urban observation station affected by traffic and residential emissions. The station is on the rooftop of the main teaching building (5 floors, ~18 m above the surface). There are no surrounding buildings higher than this building within 50 m.

2.2. Concept of the AHL/BUCT station

The station consists of four units: a field observation unit, laboratory simulation unit (under construction), calibration unit and affiliated facility unit. The field observation unit is equipped with the state-of-the-art instruments in connection to atmospheric trace gases, aerosol particle size and mass concentrations, cluster and aerosol particle chemical composition on the levels from molecular size to micrometer size. It also includes a weather station to continuously measure meteorological parameters. As an extended facility, an OnLine *in vitro* Cell Exposure Chamber (OLCEC) for toxicity studies is under construction and will be available in December 2020. The calibration unit includes an aerosol particle calibrator which can produce, dilute, and select aerosols from 1 nm to 1000 nm for particle size and number concentration, and mass concentration calibrations, and a trace gas calibrator to generate sub-ppbv to ppbv level of standard trace gases and VOCs. The affiliated facilities unit includes a vacuum system, zero air generator and cylinders, from which the pipelines go to each laboratory, a data integration and backup system and an uninterruptible power source (UPS).

All instruments, except the weather station and sampling inlets, are in temperature-controlled laboratories on the northwest part of the fifth floor. The distribution of the instruments and the details are shown in Figure 2 and Table 1. Briefly, Thermal Desorption Atmospheric Pressure Interface High Resolution Chemical Ionization Mass Spectrometer (TD-API-HR-CIMS), Atmospheric Pressure Interface Long-Time-of-Flight Chemical Ionization Mass Spectrometer (API-LToF-CIMS) (Jokinen et al., 2012), Particle Size
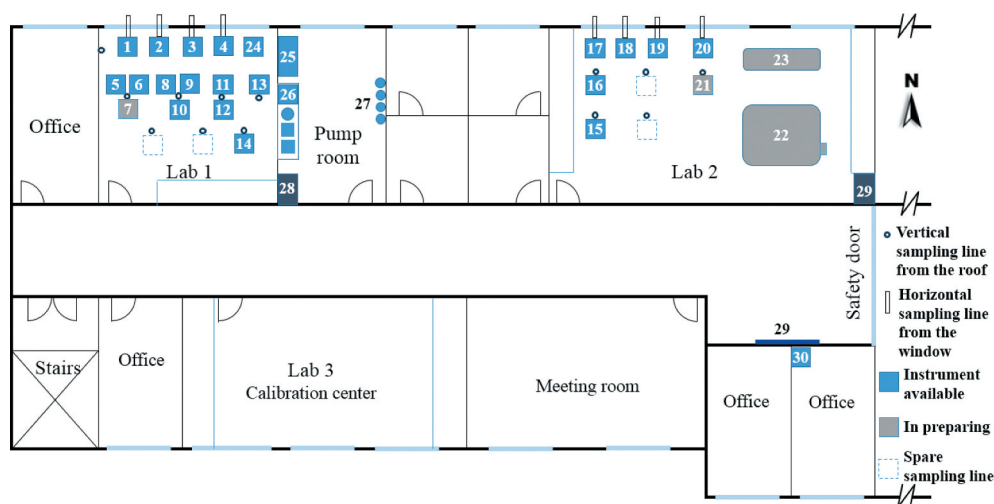

Figure 2. The vertical view of the laboratory and instruments numbered as the same as that in Table 1.

Table 1. The main instruments at AHL/BUCT Station.

No.	Instruments	Manufacturer	Targeted parameters	Time resolution	Available time
1	Thermal Desorption- Atmospheric Pressure Interface-High Resolution-Chemical Ionization Mass Spectrometer(TD-API-HR-CIMS)	Custom made by Tsinghua University	Particle composition (3–150 nm, m/z 1–1000 amu)	1 h	May 2019
2	Atmospheric Pressure Interface-Long Time-Of-Flight-Chemical Ionization Mass Spectrometer (API-LToF-CIMS)	Aerodyne	H_2SO_4, $(H_2SO_4)_n$, HOMs (m/z 1–1000 amu)	1 min	Feb 2018
3	Particle Size Magnifier (PSM)	Airmodus	1–3 nm particle size distribution	2 min	Feb 2018
4	Neutral cluster & Air Ion Specter (NAIS)	Airel Ltd,	0.8–40 nm ion and particle size distribution	1 s	Feb 2018
5	Trace Gas Analyzer (TGA)	42i-Y, 42i-TL, 43i-TLE, 48i-TLE, 49i, Thermo Fisher	NO_y, NO/NO_2, SO_2, CO, O_3	5 min	Feb 2018
6	Single Photon Ionization Mass Spectrometer (SPI-MS)	SPI-MS-3000, Guangzhou Hexin Instrument Co., Ltd	VOCs (m/z 40–300 amu)	3 min	Feb 2018
7	Vocus-Proton Transfer Reaction Mass Spectrometer (Vocus-PTRMS)	Aerodyne	VOCs, OVOCs (m/z 1–1000 amu)	1 s	June 2020
8	Time-of-Flight Aerosol Chemical Speciation Monitor (ToF-ACSM)	Aerodyne	SO_4^{2-}, NO_3^-, NH_4^+, Cl^-, OA	2 min	Feb 2018
8	Differential Mobility Particle Sizer (DMPS)	Custom made, University of Helsinki	6–760 nm particle size distribution	5 min	Apr 2018
10	Aethalometer	AE33-7, Magee	BC	1 min	Feb 2018
11	Particle Size Distribution (PSD)	Custom made by Tsinghua University	3–10,000 nm particle size	5 min	Feb 2018
12	Aerodynamic Particle Sizer (APS)	3321, TSI	500 nm–10,000 nm	5 min	May 2018
13	OC/EC Analyzer	Model 4, Sunset	OC, EC	1 h	Oct 2018
14	Taper Element Oscillating Microbalance (TEOM)	1405-DF, Thermo Fisher	$PM_{2.5}$, PM_{10}	5 min	Feb 2018
15	X-ray Heavy Metal Analyzer (XHMA)	XHAM-2000A, SailHero Environmental Protection	Heavy metals (Si, K, Ca, Ti, V, Cr, Mn, Fe, Co, Ni, Cu, Zn, Ga, As, Se, Ag, Cd, Sn, Sb, Ba, Hg, Tl, and Pb)	1 h	Nov 2018
16	Monitor for AeRosols and Gases in ambient Air (MARGA)	2060 R, Metrohm Process Analytics	SO_4^{2-}, NO_3^-, NH_4^+, Cl^-, K^+, Na^+, Ca^{2+}, Mg^{2+}, SO_2, HCl, HONO, HNO_3, NH_3	1 h	Sep 2019
17	Diethylene Glycol-Scanning Mobility Particle Sizer (DEG-SMPS)	Custom made by Tsinghua University	1–6 nm particle size distribution	5 min	May 2018
18	Green Gases Analyzer (GGA)	G2311-f, PICARO	CO_2, CH_4, H_2O	0.1 s	Dec 2019
19	Long Optical Path Absorption Photometer (LOPAP)	Custom made by Institute of Chemistry, CAS	HONO	1 min	Feb 2018
20	Filter Inlet for Gases and AEROsols API-LToF-CIMS (FIGAERO-API-LToF-CIMS)	Aerodyne	Particle-phase and gas-phase composition (m/z 1–1000 amu)	1 h	Nov 2019
21	OnLine Cell Exposure Chamber (OLCEC)	Custom made by BUCT	In vitro toxicity of air pollutants	-	Aug 2020

(Continued)

Table 1. (Continued).

No.	Instruments	Manufacturer	Targeted parameters	Time resolution	Available time
22	Quartz Indoor Smog Chamber (QISC)	Beijing Convenient Environment Tech Co. Ltd.	Chemical reaction mechanism and kinetics, 10 m^3	-	Aug 2020
23	Photochemical Flow Tube Reactor (PCFTR)	Beijing Convenient Environment Tech Co. Ltd.	Chemical reaction mechanism and kinetics, 250 L	-	Aug 2020
24	Weather station data acquisition system	Vaisala (AWS310, PWD22, CL51), Metcon	WS, WD, T, P, RH, Precipitation, Visibility, PBL, Cloud height, Cloud coverage, UVA, UVB, Global radiation, Diffusion radiation, Net radiation, J_{NO2}	1 min	Feb 2018
25	Vacuum pump	MM1142BV, Mink		-	Feb 2018
26	Zero air generator	ADCCO	High purity zero air, 250 L min^{-1}	-	Feb 2018
27	Cylinders	-	High purity N_2, O_2, He, 5% CH_4 in He, 2% O_2 in He, and air	-	Feb 2018
28	Uninterruptible Power Source (UPS)	3C20KS, Santak	20 kVA	-	Apr 2018
29	Data integration system	M6-065, Beijing F-Touch	-	-	Mar 2018
30	Data backup system	NAS, Synology	32 TB	-	Mar 2018

Magnifier (PSM) (Vanhanen et al., 2011), Neutral cluster & Air Ion Specter (NAIS) (Manninen, Mirme, Mirme, Petäjä, & Kulmala, 2016), Trace Gas Analyzers (TGA), Single Photon Ionization Mass Spectrometer (SPI-MS) (Tan et al., 2011), Vocus-Proton Transfer Reaction Mass Spectrometer (Vocus-PTRMS), Time-of-Flight Aerosol Chemical Speciation Monitor (ToF-ACSM) (Fröhlich et al., 2013), Particle Size Distribution (PSD), Differential Mobility Particle Sizer (DMPS) (Aalto et al., 2001), Aerodynamic Particle Sizer (APS), Organic Carbon/Element Carbon Analyzer (OC/EC Analyzer), Aethalometer, and Taper Element Oscillating Microbalance (TEOM) are in Lab 1, while X-ray Heavy Metal Analyzer (XHMA), Monitor for AeRosols and Gases in ambient Air (MARGA), Diethylene Glycol-Scanning Mobility Particle Sizer (DEG-SMPS) (Jiang, Chen, Kuang, Attoui, & McMurry, 2011), Long Optical Path Absorption Photometer (LOPAP) (Tong et al., 2016), Filter Inlet for Gases and AEROsols API-LToF-CIMS (FIGAERO-API-LToF-CIMS) (Yatavelli et al., 2015), OnLine Cell Exposure Chamber (OLCEC), Quartz Indoor Smog Chamber (QISC) and Photochemical Flow Tube Reactor (PCFTR) set in Lab 2.

On the roof, the weather station is in the middle of the two arrays of the sampling inlets. Two gas inlets and six aerosol inlets are over Lab 1, and other five aerosol inlets are over Lab 2. The distance between the two nearest inlets is 1.5 m to reduce the local turbulence. All the heads of the inlets on the roof are 0.5 m above the top of the skirt-walls (1.0 m) of the building. The inner parts of the sampling tubing (2.0 m long) are wrapped with heat-insulating materials to prevent water condensation in summer. A Teflon sampling tubing (BMET-S, Beijing Saak-Mar Environmental Instrument Ltd.) and $PM_{2.5}$ or PM_{10} (URG) inlet heads with polishing steel tubing are used for gas and aerosol sampling, respectively. The residence time of air mass in the sampling tubing is <10 s, while it is <6.5 s with a Reynolds number of 800 to make sure a laminar flow in the sampling tubing for aerosol sampling. For some instruments, such as TD-API-HR-CIMS, API-LToF-CIMS, FIGAERO-API-LToF-CIMS, PSM, NAIS, Nano-SMPS, and LOPAP, the ambient air is drawn through the window or wall with corresponding ~1.5 m sampling tubing to reduce the loss of sticky or reactive species. A lightning rod (5.5 m height, ESE2500, Duval Messien) is installed on the roof to protect all of these inlets from lightning strike.

2.3. Instrumentation

2.3.1. Trace gases

NO_x (NO and NO_2) and NO_y (NO, NO_2, NO_3^-, N_2O_5, HNO_3, PANs, and $RONO_2$) are measured using NO_x analyzer (42i-TL, ThermoFisher) and NO_y analyzer (42i-Y, ThermoFisher), respectively. SO_2, CO and O_3 are measured with a SO_2 analyzer (43i-TLE, ThermoFisher), a CO analyzer (48i-TLE, ThermoFisher) and ozone analyzer (49i, ThermoFisher), respectively. Volatile organic compounds (VOCs) are measured using a SPI-MS (3000 R, Hexin Mass Spectrometry) (Gao et al., 2013). Oxygen-containing VOCs (OVOCs) will be detected using a Vocus-PTRMS (Tofwerk) (Krechmer et al., 2018), which will be available in June 2020. Sulfuric acid (H_2SO_4), clusters of sulfuric acid ($H_2SO_4)_n$, $(H_2SO_4)_n(NH_3)_x(amines)_y$, nitrophenols, and highly oxygenated molecular (HOMs) with m/z in the range of 1–1000 amu are measured using a nitrate-API-LToF-CIMS (Aerodyne) (Jokinen et al., 2012; Kürten et al., 2014; Yao et al., 2018). HONO is measured using a home-made LOPAP (Institute of Chemistry, Chinese Academy of Sciences) (Tong et al., 2015, 2016). HONO is also detected by MARGA

(Metrohm). Greenhouse gases including CO_2 and CH_4 are measured using a Greenhouse Gases Analyzer (G2311-f, Picarro) based on cavity ring down spectroscopy (CRDS, Picarro).

The NO_y analyzer samples from the roof using an individual Teflon sampling tubing. The nitrate-API-LToF-CIMS and the LOPAP sample from the window to reduce the loss of sticky and/or reactive compounds. TGA for SO_2, NO_x, CO and O_3, and SPI-ToF-MS for VOCs share a heated (40 °C) Teflon sampling tubing from the roof. HONO, HCl, SO_2, HNO_3, and NH_3 measured with a MARGA are sampled from the roof using an individual sampling tubing. The details about the instruments are shown in the Supplementary Material.

2.3.2. Particle number size distribution and particulate mass

Several instruments based on different technologies are deployed to measure the particle size distribution from 1 to 10,000 nm. A PSM (Airmodus) is used to measure the size distribution of 1–3 nm particles (Vanhanen et al., 2011). 1–10 nm particles are cooperatively measured with a custom made DEG-SMPS operated by Tsinghua University. Particles from 2 to 40 nm and ions from 0.8 nm to 40 nm are measured using a NAIS (Airel Ltd) (Mirme & Mirme, 2013). Particles from 6 to 760 nm are measured with a custom-made DMPS (Aalto et al., 2001). The particles from 500 nm to 10,000 nm are measured by an APS (3321, TSI). In addition, a PSD, which integrates a nano-DMA (3085, TSI), a long DMA (3081, TSI) and an APS, is also deployed to measure the particle size from 3 nm to 10,000 nm. Using these instruments, the particles/cluster size distribution from 0.8 nm to 10,000 nm are monitored simultaneously.

Particle mass concentration, $PM_{2.5}$ and PM_{10} (Particulate Matter with aerodynamic diameter < 2.5 and < 10 μm, respectively) is measured using a TEOM (1405-DF, ThermoFisher). The $PM_{2.5}$ and PM_{10} concentrations are also downloaded from the nearest four national monitoring stations (Wanliu, Gucheng, Wanshouxigong and Guanyuan) of the China National Environmental Monitoring Center (CNEMC) for comparison.

The PSM, the NAIS, and the DEG-SPMS directly sample from the window with individual sampling tubes to reduce the loss of ultrafine particles, while the APS shares a sampling tubing and a PM_{10} inlet with the PSD from the roof, and the DMPS shares a sampling tubing and a $PM_{2.5}$ inlet with the ACSM and the Aethalometer, which will be discussed in the following section.

2.3.3. Particle composition

The bulk composition including chloride, nitrate, sulfate, ammonia and organics of non-refractory $PM_{2.5}$ (NR-$PM_{2.5}$) is measured with a ToF-ACSM (Aerodyne) (Fröhlich et al., 2013). FIGAERO-CIMS (Lopez-Hilfiker et al., 2014) is deployed to measure the molecular composition of bulk $PM_{2.5}$ and trace gases alternatively. A TD-API-HR-CIMS (Smith, Moore, McMurry, & Eisele, 2004) is deployed to measure the composition of nano-particles (3–150 nm) selected by three parallel nano-DMAs (3085, TSI). Inorganic ions including NO_3^-, SO_4^{2-}, Cl^-, NH_4^+, K^+, Ca^{2+}, and Mg^{2+} in $PM_{2.5}$ and soluble gases including SO_2, HCl, HONO, HNO_3 and NH_3 are measured by a MARGA with one-hour time resolution. Heavy metals (Si, K, Ca, Ti, V, Cr, Mn, Fe, Co, Ni, Cu, Zn, Ga, As, Se, Ag, Cd, Sn, Sb, Ba, Hg, Tl, and Pb) in $PM_{2.5}$ are measured with an XHMA. Black carbon (BC) is measured using an Aethalometer (Magee). Organic carbon (OC) and element carbon (EC) are semi-continuously measured using an OC/EC analyzer (Model 4, Sunset) based on thermal optical transmission (TOT) method.

The ACSM and the Aethalometer share one sampling tubing from the roof after cutting particles with diameter larger than 2.5 μm. Before sampling by the instruments, the air is dried using a Nafion dryer (MD-700-24 F-3, Perma Pure). The OC/EC analyzer, the XHMA and the TEOM sample from the roof using the individual sampling tubing. $PM_{2.5}$ inlets are installed for the OC/EC and the XHMA, while a PM_{10} inlet is used for the TEOM. The FIGAERO-CIMS samples from the window for gas measurement, while from the roof with a $PM_{2.5}$ inlet for particle measurement. The TD-HR-CIMS samples from the window to reduce the loss of small particles.

2.3.4. Meteorological parameters

Wind speed (WS), wind direction (WD), atmospheric pressure (*P*), temperature (*T*), relative humidity (RH), precipitation, visibility, global radiation, diffused radiation, net radiation, and ultraviolet radiation (A and B) are measured with an Automatic Weather Station (AWS310, Vaisala). Cloud height and vertical visibility are measured based on the echo time of the exciting laser (910 nm) and cloud coverage is measured by the moving integration algorithm within 30 min using a ceilometer (CL51, Vaisala). Planetary boundary layer (PBL) height can also be inferred from the backward scattering signals. Horizontal visibility is measured by a visibility sensor based on forward scattering signal (PWD22, Vaisala). The photolysis rate (J_{NO2}) is measured via a continuous measurement of the actinic flux in the wavelength range of 285–375 nm using a J_{NO2} filter-radiometer (2-pi-J_{NO2} radiometer, Metcon).

2.3.5. Data backup system

All the instruments have independent data acquisition system and computers. We have developed a data integration and backup system for routine data quality check and data backup. The real-time raw data are automatically uploaded to a network-attached storage (NAS, Synology) per hour. The total capacity of the hard disk array is 32 TB. A custom-made data integration system can selectively read the data, such as meteorological parameters, concentration of trace gases, PM mass concentration and composition, from the NAS and show the corresponding plot on a screen.

2.3.6. Affiliated facilities

Dried zero air is needed by several instruments such as the nitrate-LToF-CIMS, the PSM, and the DMPS, while dried compressed air is required for drying aerosol before going into the ACSM, the Aethalometer, the DMPS, the PSD and so on. A pure air generator system, containing an oil-free air compressor (SLPJ-37B, ANEST IWATA), a gas tank (0.3 m^3 @ 8 atm), a low temperature dryer (CAPITOR), and zero air generator (737–15, AADCO), is in the pump room (Figure 2). The maximum output flow rate of the compressor and the zero air generator is 405 lpm and 250 lpm, respectively. Dried compressed air (with dew point of −51°C) is branched into the zero air generator and pipelines into the laboratories. Thus, both dried zero air and compressed air are available in each laboratory. An oil-free vacuum pump (MM1142BV, Mink) is in the pump room to provide vacuum condition in each laboratory. Two 20 KVA UPS (Santak) are installed in the pump room and Lab 2, respectively. All the instruments in Lab 1 and Lab 2 can run for ~1 hour in the case of interruption of power supply. The gas cylinders are in the pump room.

2.4. Data quality control

Data quality is very important in the continuous observations. The experiment log for each instrument is recorded every day including responsible person and instrument status which is updated weekly. Science meeting about data quality control is held weekly. The setup of the calibration system is shown in Figure S1 and the corresponding calibration protocols are shown in the Supplementary Material.

Figure 3(A-F) show the concentrations of SO_2, CO, NO_2, O_3, $PM_{2.5}$ and PM_{10} measured at our station and the corresponding mean concentrations of the four nearest surrounding national monitoring stations from Feb 2018 to Feb 2019. Overall, these pollutants show similar variations and the comparable concentrations. Figure S2 shows the corresponding scattering plot. The slope and the correlation coefficient (R) between the measured concentration at the AHL/BUCT Station and the surrounding values are 0.95 and 0.88 for SO_2, 0.98 and 0.93 for CO, 0.90 and 0.93 for NO_2, 0.95 and 0.96 for O_3, 0.80 and 0.97 for $PM_{2.5}$, 0.78 and 0.92 for PM_{10}, respectively. The trace gas results at our station are closely consistent with the surrounding stations, while the TEOM at our station slightly underestimates the PM concentration when compared with the surrounding stations.
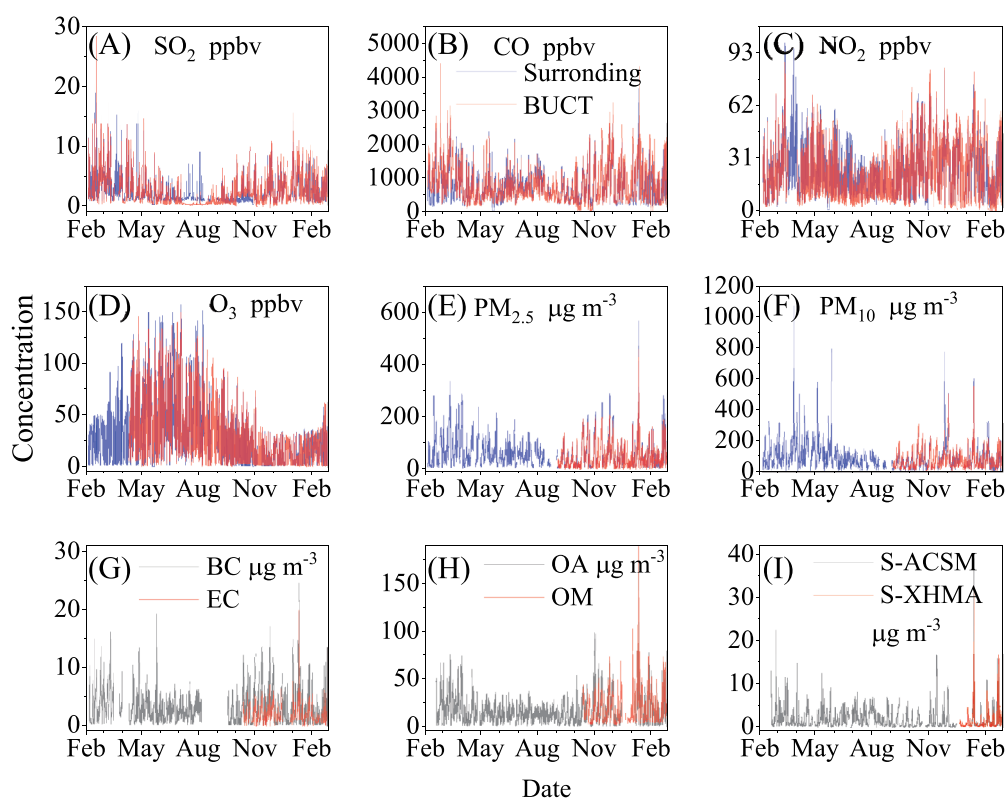
Figure 3. Comparison of the concentration of selected pollutants (A)-(F) measured at the AHL/BUCT Station with the mean concentration of the four nearest surrounding national monitoring stations from Feb 2018 to Feb 2019, (G) BC and EC concentration measured with the Aethalometer and the OC/EC Analyzer, respectively, (H) OA and OM (OM = OC×1.8) concentration measured with the ACSM and the OC/EC Analyzer, respectively, and (I) chloride concentration measured by the ACSM and the XHMA, respectively.

To further check out the data quality, the concentrations of a same or similar pollutant measured by different method are also routinely compared. As shown in Figure 3G, the concentration of EC measured by the OC/EC Analyzer well tracks the variation of BC measured with the Aethalometer. The slope is 0.52 along with a correlation coefficient of 0.98. The calculated organic matter (OM = OC×1.8) measured by the OC/EC Analyzer also well correlated with the OA measured with the ACSM (Figure 3H). The slope is 1.01 with a correlation coefficient of 0.96. The sulfide measured by the XHMA correlates well with that measured by the ACSM with a slope of 0.82 and correlation coefficient of 0.91 (Figure S1). Although some deviations are observed among the absolute values for these parameters due to different form, OC and EC show good correlations with OA and BC, respectively. In the future, intercomparisons will be further carried out between different instruments in our laboratory, such as VOCs concentration measured by the SPI-MS and the PTR-MS, the NO concentration measured by the NO_x and NO_y analyzers, the HONO concentration measured by the LOPAP and the MARGA and the particle size distribution measured by different instruments. In addition, we are also looking for the opportunity to do intercomparison with other laboratories and companies.

3. On observational results

3.1. Overview of the data set

The continuous observations started on February 2018 with the instruments (Table 1) from BUCT, Tsinghua University and Chinese Academy of Sciences (Institute of Chemistry, Research Center for Eco-Environmental Sciences and Institute of Atmospheric Physics). Around 20 instruments were deployed at the AHL/BUCT Station from February 2018 to January 2019. Besides the long-term and continuous observation, two intensive campaigns have also been cooperatively organized with Fudan University from Feb 1 to April 11, 2018 and Nanjing University of Information Technology from October 20, 2018 to March 13, 2019. Overall, the data coverage varied from 40% to 100% depending on instruments due to instrument calibrations, maintenance, and other deployments. The total data size is around 600 GB for one year's observation. The details are shown in Table 2.

3.2. General feature of the air quality
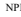
Table 3 summarizes the air quality index (AQI) and the classification of pollution events from February 2018 to January 2019. The annual mean $PM_{2.5}$ concentration was 57.7 μg m^{-3}, which was close to that in 2017 Beijing (Cheng et al., 2019). In 2018, 31.8 % of days were in unhealthy and even worse air quality (with AQI >100). At the same time, as the corresponding primary pollutant, $PM_{2.5}$, PM_{10}, O_3 and NO_2 dominated 77%, 19%, 3 % and 1 % of the pollution days (with AQI >100), respectively. High frequency of heavy pollution events (with AQI > 150) accompanied with high $PM_{2.5}$ concentration occurred from November to April (mainly in heating season) (Figure 4). The frequency of hourly $PM_{2.5}$ concentration higher than 75 μg m^{-3} with RH lower than 90% was 47% from November to April, while it was 34% in other months. This is the typical feature that pollution event usually happens in autumn and winter Beijing (An et al., 2019).

Table 2. Overview of the main data set from February 2018 to January 2019.

Instruments	PSM	DMPS	NAIS	ToF-ACSM	TGA	Ceilometer	Automatic weather station	PSD	DEG-SMPS	LOPAP	SPI-MS	Aethalometer	TEOM	API-LTOF-CIMS	APS	OC/EC Analyzer	XHAM
Duration	2018/2/1-2019/1/31							2018/2/1-2018/5/1; 2018/10/20-2019/1/31		2018/2/1- 2018/7/1; 2018/9/30- 2019/1/31	2018/2/1-2018/8/7; 2018/9/21-2019/1/31		2018/2/27- 2019/1/31	2018/5/14- 2019/1/31	2018/5/1- 2019/1/31	2018/10/20- 2019/1/31	2018/11/3- 2019/1/31
Sampling time (days)	365	245	365	365	365	365	365	211	211	274	320	320	339	263	276	104	90
Data size (MB/day)	0.05	0.08	3.00	19.5	0.01	90.0	50.0	9.0	0.05	12.0	0.04	0.6	0.05	5120.0	0.00	0.01	178.0
Total Data size (GB)	0.01	0.02	0.9	6.6	0.003	31.4	17.8	2.6	0.01	0.003	0.01	0.2	0.02	535.0	0.00	0.001	14.1
Percentage of effective data (%)	71	87	81	95	96	98	100	77	64	97	80	87	98	41	40	95	90

Table 3. The calendar of air quality index and the classification of events from February 2018 to January 2019.

		1	2	3	4	5	6	7	8	9	10	11	12	13	14	15	16	17	18	19	20	21	22	23	24	25	26	27	28	29	30	31
																						Date										
	Feb	67	35	28	37	32	61	63	69	90	41	64	52	80	43	62	105	105	148	185	72	51	44	48	63	75	159	219	133			
	Mar	48	99	217	135	92	65	64	61	136	165	83	183	289	293	69	57	82	135	101	44	78	114	146	117	76	155	245	388	115	68	128
	Apr	221	283	78	34	91	78	52	68	112	96	50	78	64	122	66	104	142	144	170	173	102	35	41	45	61	118	111	129	196	62	
	May	125	45	50	87	179	121	102	68	86	122	105	190	72	168	95	147	64	60	78	59	82	105	142	107	111	140	89	188	46	56	97
	Jun	91	120	92	76	110	116	71	52	52	60	88	125	77	66	130	111	77	126	92	79	91	90	128	121	109	183	57	40	71	108	
Month	Jul	80	72	85	112	126	92	72	81	103	49	43	44	59	80	99	45	27	105	91	114	107	69	81	27	36	48	68	94	111	116	118
	Aug	109	130	100	122	67	53	86	41	67	102	69	74	66	41	37	53	100	46	40	51	44	47	51		90		114		44		62
	Sep		58	46	26	37	40	25	29	55	66	71	65	109	128	39	30	42	50	53	64	48	27	29	27	47	52	85	76	22	23	
	Oct	31	32	37	67	105	33	35	39	3	25	32	63	107	179	200	82	54	49	60	86	144	168	38	70	112	45	34	37	24	33	48
	Nov	70	151	210	107	29	33	52	91	63	37	70	126	222	274	92	33	67	67	77	71	44	56	92	118	117	252	192	115	104	120	
	Dec	165	233	193	61	75	37	36	38	62	78	53	54	41	71	118	101	53	52	60	81	89						50	41	28	31	56
	Jan	53	65	163	49	31	85	57	31	59	104	136	241	159	154	54	60	66	86	34	34	53	60	47	80	35	35	90	52	135	74	33

Note: NPF · Haze · Transition · Undefined · The numbers mean the daily air quality index (AQI)

$AQI = \max(IAQI_1, IAQI_2, \ldots IAQI_n)$, $IAQI_P = \frac{IAQI_{High} - IAQI_{Low}}{C_{High} - C_{Low}}(C_P - C_{Low}) + IAQI_{Low}$, where $IAQI$ is the AQI for a given pollutant; C_P is the pollutant concentration; C_{High} and C_{Low} are the concentration breakpoints higher and lower than C_P, respectively; $IAQI_{High}$ and $IAQI_{Low}$ are the index breakpoints corresponding to C_{High} and C_{Low}.

In addition to frequent occurrence of air pollution dominated by fine particles, new particle formation (NPF) events were vigorous throughout the year. Table 3 summarizes the classification of the pollution and NPF events day by day according to the method proposed by Dal Maso et al. (2005) and modified to fit polluted urban environments. Namely, NPF event was identified by the appearance of cluster mode particles (1–3 nm) followed by further growth into nucleation mode particles (3–25 nm). Haze was identified by the PM$_{2.5}$ concentration higher than 75 μg m^{-3} with the relative humidity less than 90% at least lasting for 1 hour per day. The annual NPF occurrence was 49.4%. In February, April, May, June, July, September, October, and December, the occurrence of NPF exceeded 50% (Figure 4C). This highlights the active secondary transformation of pollutants in Beijing. However, it is still an open question that why new particle formation or secondary transformation of pollutants is more efficient in winter under polluted urban environment (Kulmala, 2015; Kulmala et al., 2017). This is also one of our research interests in the future.

3.3. Variation of meteorological conditions

Figure 5 summarizes the typical meteorological parameters throughout one year of observations. High temperature, high RH and low pressure usually occurred from May to October, and vice versa in other months. 42% of hourly visibility was lower than 10 km with RH less than 90%. This is comparable to the frequency (41%) of hourly PM$_{2.5}$ concentration higher than 75 μg m^{-3} and RH lower than 90%. Although the PM$_{2.5}$ concentration was significantly lower in summer than in other seasons (Figure 4), high RH was favorable for decreasing of the visibility in summer. Therefore, no significant difference for the frequency of low visibility among different seasons (43% from November to Jan vs 41% from April to October) was observed.

As shown in Figure 1, the half-basin terrain feature of Beijing helps the formation of stagnant weather conditions. The stagnant weather, with wind speed lower than 1 m s^{-1} and the mixed layer height (MLH) lower than 500 m, occurred with a high probability in every season (Figure 5E). Because of intensive emissions of air
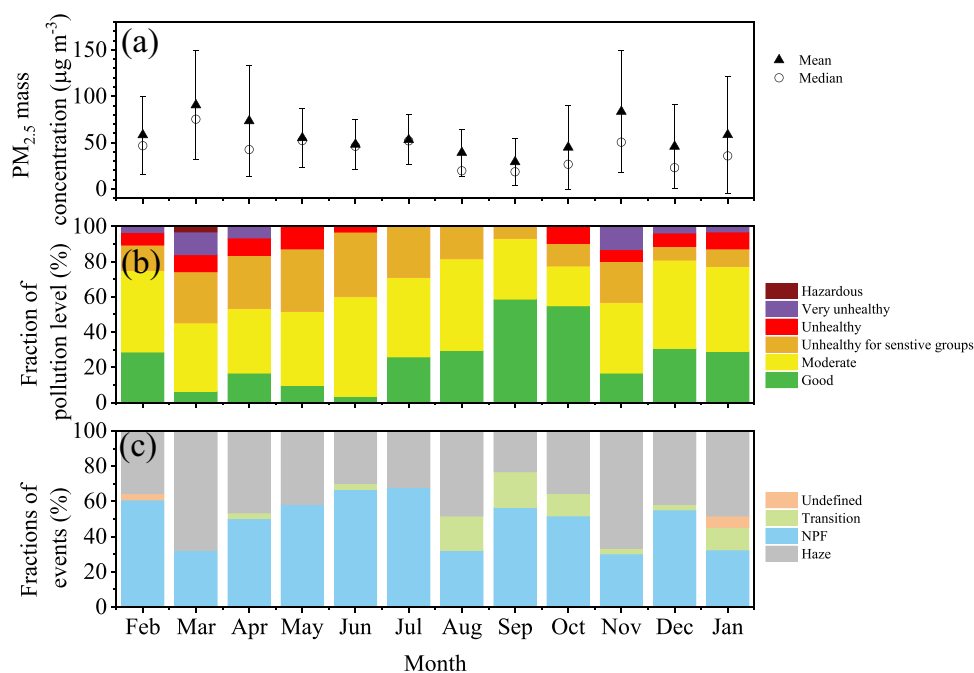
Figure 4. Monthly distribution of (A) PM$_{2.5}$ concentration, (B) air pollution levels defined in the light of AQI and (C) the mean frequency of events classed as the same as that in Table 3 from February 2018 to January 2019.

pollutants in the surrounding areas, the meteorological conditions are the controlling factor determining the air quality in Beijing. In particular, the stagnant weather conditions, such as low wind speeds (< 2 m s^{-1}) from south directions and low MLH, usually become the sufficient and necessary conditions of pollution events in Beijing. The pollution level (AQI) was greatly affected by the air parcels from the local and south regions, bringing high concentrations of pollutants from south directions to Beijing, especially with low wind speeds (Sun et al., 2010) due to the distribution of the megacity and industry in the NPC region.

3.4. Monthly chemical composition of fine particles

Figure 6 shows the composition of non-refractory-PM$_{2.5}$ (NR-PM$_{2.5}$) measured using the ToF-ACSM and BC from February 2018 to January 2019. As shown in Figure 6A, air pollution occurred periodically with a cycle of 5–7 days (Guo et al., 2014; Wang et al., 2016). Similar to the monthly distribution of the AQI (Figure 4), concentrations of NR-PM$_{2.5}$ during the period from November to April were significantly higher than during the rest of the year. All of the NR-PM$_{2.5}$ components, including nitrate, sulfate, ammonium, chloride, OA and BC, showed high concentrations in the heating season (from October 15 to March 15) compared with the non-heating season (Figure 6B). Organic aerosol contributed from 34% to 48% of the monthly mean of NR-PM$_{2.5}$, followed by nitrate (20–38%), sulfate (12–22%), ammonium (11–16%) and chloride (<5%). In particular, nitrate and organic aerosol showed significantly
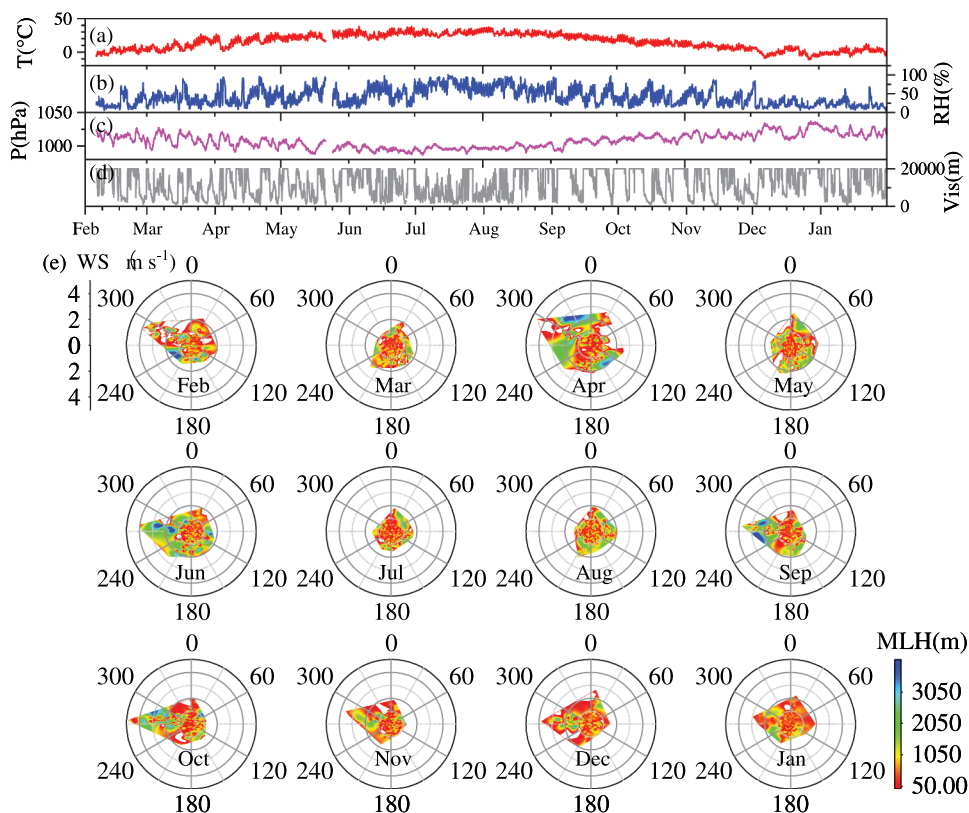
Figure 5. Meteorological parameters from February 2018 to January 2019.

higher contribution to the NR-PM$_{2.5}$ during the heating season than during the non-heating season. These results imply the importance to reduce NO$_x$ and volatile organic compounds emission in Beijing and surrounding areas.

Figure 7 shows the distribution of NR-PM$_{2.5}$ mass concentrations in the two-dimensional space of wind speed and wind direction. The strong northwest or west wind resulted into low mass loading of the NR-PM$_{2.5}$, while the weak wind (< 2 m s^{-1}) from the southwest, south and southeast directions led to high mass concentrations for all these NR-PM$_{2.5}$ components. This can be explained by the industrial distribution in south related directions and the terrain of Beijing (Fig. S1). Under stagnant meteorological conditions, the southern air masses usually bring high concentration of air pollutants along Taihang Mountain to our observation site (Sun et al., 2015). When the air masses reach to Yanshan Mountain, the blocking role of the mountains lead to high concentration of pollutants from northeast direction wind (Quan et al., 2020). Although the mass concentrations showed a similar dependence on the wind field among different components of NR-PM$_{2.5}$, the relative contributions showed obvious different responses to the wind field among different components because the variation of particle composition at different PM pollution levels (Figure. S3). High fractions of nitrate, sulfate, and ammonium were connected to the air parcels from the southwest and southeast directions on pollution days, while high OA fractions were highly associated with air masses from the
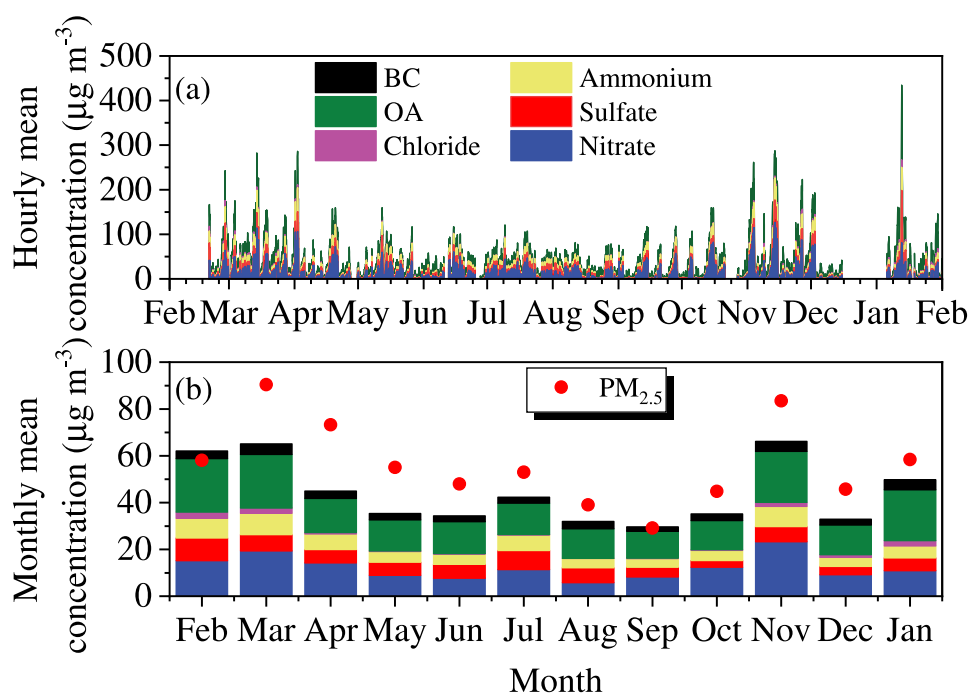
Figure 6. The composition of non-refractory-PM$_{2.5}$ from February 2018 to Jan 2019.

north and northwest directions on relatively clean days. High fractions of sulfate, ammonium, and OA sometimes were observed for the air masses from the northwest direction even at high wind speeds (> 4 m s^{-1}). This implies the regional characteristic of fine particle formation in China. In the future, the dependence of particle composition on wind direction will be further analyzed in terms of source apportionment and the potential source contribution function (PSCF) analysis.

## 3.4. Evolution of air quality from clean to pollution days

Figure 8 shows a typical case of shifting from NPF days (clean days) to pollution days. Before of 6:00 am in March 19, the very low MLH and wind speed resulted into high concentration of PM$_{2.5}$ (> 100 μg m^{-3}), whose diameter was around 150 nm. In the early morning, a breeze in the following ~3 hours from the northeast direction was accompanied with a gradual increase of MLH (Figure 8A), leading to the dispersion of accumulated pollutants both horizontally and vertically. At the same time, new particle formation supported by high concentrations of H$_2$SO$_4$ (Figure 9C) and explosive growth of the particle number concentration (Figure 8B) started along with the photochemistry, lasting until 2:00 pm. Then, the weak wind (~ 1 m s^{-1}) shifted to the southeast direction, leading to a slight increase of the concentration of large particles (~ 100 nm) and decreased particle growth until 6:00 pm. Finally, the air parcel from southwest direction along with a decrease in MLH led to an increase of the PM$_{2.5}$ concentration again in the night. In the second day, a similar sequence of processes occurred. However, the continuous weak winds from south direction resulted into the building up of a long-term pollution event
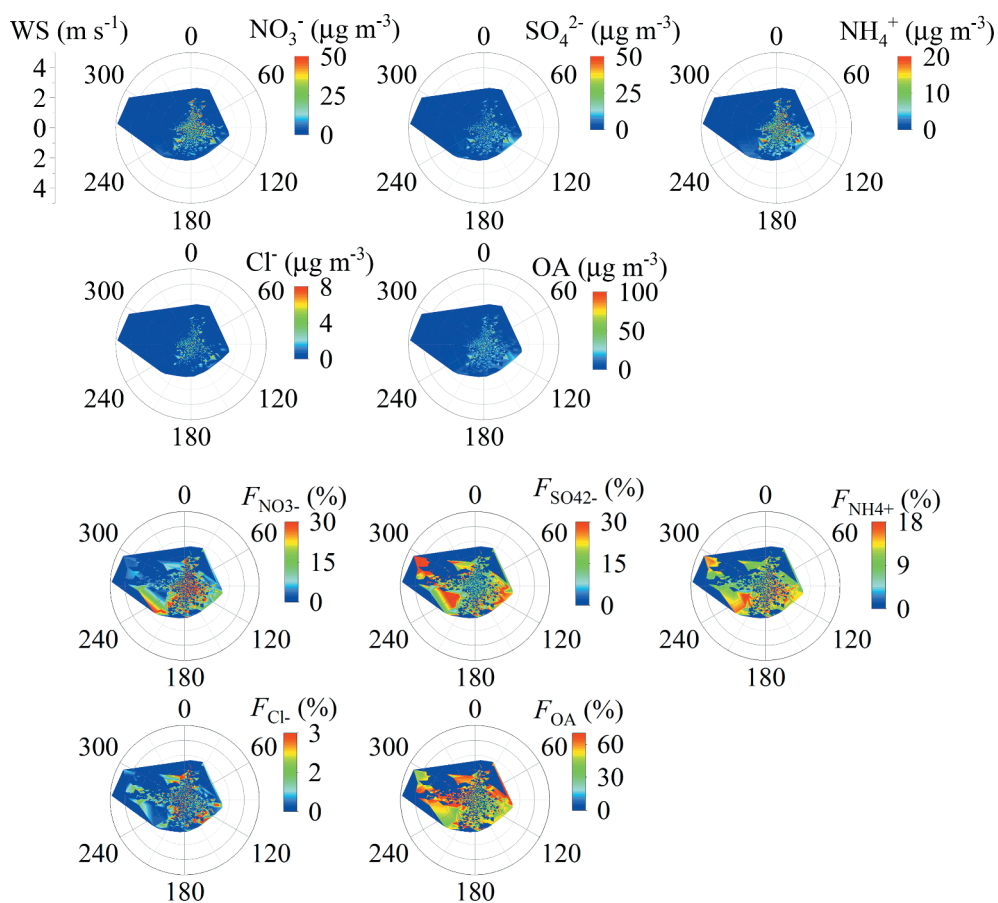
Figure 7. The dependence of NR-PM$_{2.5}$ concentration and composition on wind direction and wind speed from Feb 2018 to Jan 2019.

until the noon of Mach 24. The strong winds and broken of inversion layer resulted in a clean day at noon of Mach 24. Many gaseous pollutants, including SO$_2$, CO, and VOCs, SVOCs, IVOCs, LVOCs, and ELVOCs (Figure 9), showed similar variations as PM$_{2.5}$, whereas H$_2$SO$_4$ and O$_3$ concentrations were more sensitive to the sunlight.

As shown in Figure 8C, the composition of NR-PM$_{2.5}$ in the NPF events was obviously different from that in the pollution events. The contribution of organic component to the NR-PM$_{2.5}$ was obviously higher in the NPF events than that in pollution events, while inorganic components, including nitrate and ammonium, contributed more to NR-PM$_{2.5}$ in polluted days. This is consistent with previous findings about the chemical composition of NR-PM$_{1.0}$ observed at difference pollution levels (Sun et al., 2015). At the very beginning of the NPF events, the fraction of nitrate usually fell down to the lowest value (Figure 8C), followed by its gradual increase along with the particle growth (Figure 8B). This implies a possible role of nitrate in particle growth, which is required to be clarified in the future. It should be noted that the detectable size of the ToF-ACSM is much larger than those of particles involved in NPF. It is urgent to directly measure the composition of particles from the cluster mode to the nucleation mode to understand the birth and growth of new particles. Therefore, we have deployed
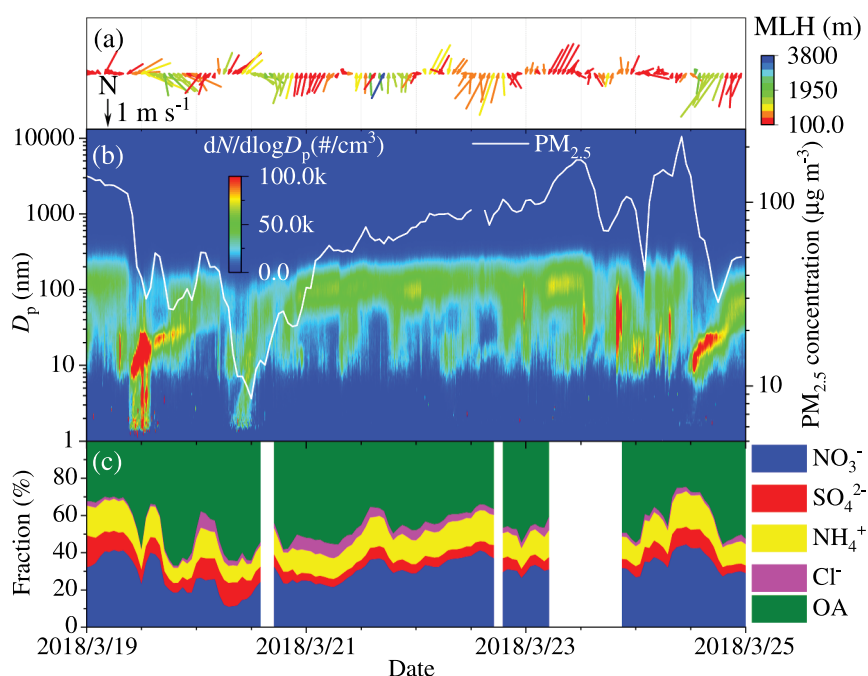
Figure 8. Evolution of (A) weather conditions, (B) particle size distribution and PM$_{2.5}$ mass concentration, and (C) composition of NR-PM$_{2.5}$ from March 19 to 25, 2018.

several chemical ionization mass spectrometers, such as nitrate-CIMS, TD-nitrate-CIMS, and FIGAERO-LToF-CIMS, to answer this challengeable question. The relevant work is still ongoing.

As shown in Figure 9B, concentrations of VOCs during the NPF days were significantly lower than those during the polluted days. The same pattern was observed for oxygenated organic molecules (OOMs) (Figure 9C), although their concentration were two orders of magnitude lower than those of VOCs. During the first NPF event (Figure 9), OOMs showed a decreasing trend, while it increased slightly during the second NPF event. This means that nucleation should be independent of the OOMs concentration. In polluted days, however, accumulation of OOMs was prominent as shown in Figure 9. This implies that OOM should play an important role in particle growth in polluted days. The details will be discussed in a separate work in the future. Overall, these results demonstrate that we can understand atmospheric processes from nucleation to haze formation based on our comprehensive measurements. The meteorological parameters, gas phase precursors for particle formation, particle size distribution, and particle concentration have been well characterized. More general and universal rules about air pollution in megacity Beijing will be investigated on the evidence of continuous and comprehensive observations in the future.

4. Conclusions

Rapid urbanization and industrialization have led to very serious and complex urban air pollution in China and in other developing countries. This requires a full
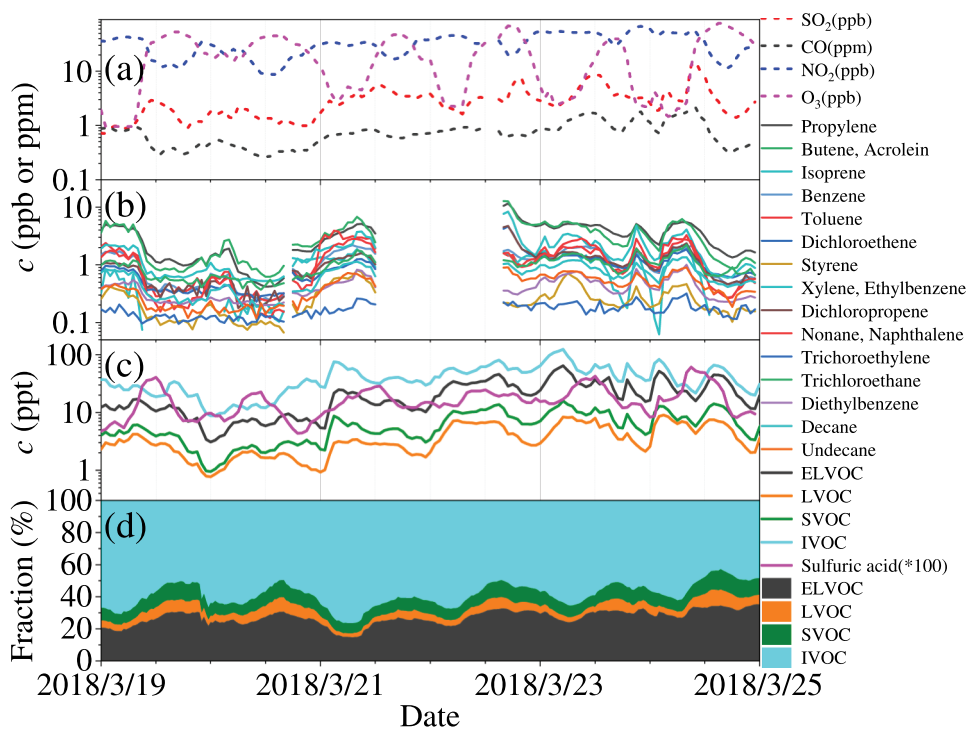
Figure 9. Concentrations change of (A) SO$_2$, CO, NO$_2$, O$_3$, (B) VOC, (C) ELVOC, LVOC, SVOC, IVOC and H$_2$SO$_4$, (D) relative fraction of SVOC, IVOC, LVOC and ELVOC, and (E) the mass defect graph of oxygenated organic molecules measured by a nitrate-ToF-CIMS.

understanding on the sources of crucial air pollutants, formation mechanism of secondary pollutants and possible impacts of air pollution on human health, climate change and ecosystem in the hot spots of air pollution in the world. In this work, we described the details about our newly constructed AHL/BUCT Station. The aim of the stations is to understand complex urban atmospheric environment in Beijing mega-city. The station, equipped with the state-of-the-art facilities in an atmospheric environment, consists of a field observation unit, laboratory simulation unit, calibration unit, and affiliated facility unit. The preliminary results from 2018 to 2019 demonstrate that our observation station is capable of continuously measuring plenty of parameters in connection to meteorological conditions, atmospheric trace gases, aerosol particle size and mass concentrations, and finally particle chemical composition from molecules to micrometer-sized aerosol particles. The facilities will provide us powerful tools to fully understand the mechanism of aerosol formation and growth, the causes of complex urban air pollution, and the impacts on human health, climate change, and ecosystems. The AHL/BUCT observatory is able to contribute to the global observatory (Kulmala, 2018) with its comprehensive data. The huge size of dataset and the large number of variables for our long-term observation require special statistical tools such as cluster analysis, positive matrix factor analysis, and artificial intelligence to answer the scientific questions mentioned above in the future like the process of any other big data. At the start of the AHL/BUCT Station, we are open mind to corporate with the

scientists at home and abroad, such as University of Helsinki, Finland, Tsinghua University, Fudan University, and Nanjing University of Information Science & Technology, Chinese Academy of Sciences (Institute of Chemistry, Research Center for Eco-Environmental Science, Institute of Atmospheric Physics) and Karlsruhe Institute of Technology, Germany. We unreservedly share the data among our collaborators and also welcome the corporation with scientists whose research interests are complementary with ours.

Disclosure statement

No potential conflict of interest was reported by the authors.

Notes on contributors

Dr. Yongchun Liu is a full professor of Beijing University of Chemical Technology. He received his Ph.D degree from Chinese Academy of Sciences in 2008, then worked as a research scientist at Research Center for Eco-Environmental Sciences, Chinese Academy of Sciences until 2017. His research interests focus on atmospheric chemistry and its environmental impacts, such as the heterogeneous reaction mechanism and kinetics of trace gases on ambient relevant particle matter, chemical aging and toxicological evolution of carbonaceous aerosols, source apportionment of air pollutants and so on. He has published more than 90 peer-reviewed papers.

Dr. Federico Bianchi, born in Bergamo, Italy, in 1984, graduated in chemistry from University of Milan. After working for four years as a Marie Curie student at the CLOUD project in CERN and at the Paul Scherrer Institute, he received his Ph.D. in atmospheric chemistry from the Eidgenössische Technische Hochschule (ETH) Zürich (2014). In 2017, he received the Arne Richter Award for Outstanding Early Career Scientists given by the European Geosciences Union. After being awarded with an ERC Starting Grant, he was appointed as Associate Professor on atmosphere and cryosphere interactions at the University of Helsinki. His research interests are the formation of new particles in extreme environments, from pristine free troposphere to polluted megacities. Currently, his group is focusing on understanding preindustrial atmosphere and the influence of biogenic highly oxygenated organic molecules on aerosol formation.

Dr. Markku Kulmala, Academy Professor, directs the Institute for Atmospheric and Earth System Research (INAR) and has served as Professor at the University of Helsinki since 1996. Kulmala also acts as coordinator for the Centre of Excellence, appointed by the Academy of Finland the first time in 2002 and the Digital Belt and Road Program International Center of Excellence at the University of Helsinki. Previously, he has directed the Nordic Center of Excellence, appointed by Nordforsk (CRAICC), which is the largest joint Nordic research and innovation initiative to date, aiming to strengthen research and innovation regarding climate change issues in the Nordic and high-latitude regions. He has received several international awards such as the Smoluchovski Award (1997), the International Aerosol Fellow Award (2004), the Wilhelm Bjerkenes medals (2007), Fuchs Memorial Award (2010), Litke Gold Medal of the Russian Geographical Society (2015), the honorary title of Academician of Science (Finland and China), Wihuri International Prize 2017, Distinguished Visiting Fellow (IIASA), and World Academy of Sciences fellow.

ORCID

Yongchun Liu (iD) http://orcid.org/0000-0002-6758-2151
Douglas R. Worsnop (iD) http://orcid.org/0000-0002-8928-8017
Tuukka Petäjä (iD) http://orcid.org/0000-0002-1881-9044
Markku Kulmala (iD) http://orcid.org/0000-0003-3464-7825

Data availability statement

The data that support the findings of this study are available from the corresponding author (liuyc@buct.edu.cn) upon reasonable request.

References

Aalto, P., Hämeri, K., Becker, E., Weber, R., Salm, J., Mäkelä, J. M., . . . Kulmala, M. (2001). Physical characterization of aerosol particles during nucleation events. *Tellus B*, *53*(4), 344–358.

An, Z., Huang, R.-J., Zhang, R., Tie, X., Li, G., Cao, J., . . . Ji, Y. (2019). Severe haze in northern China: a synergy of anthropogenic emissions and atmospheric processes. *Proceedings of the National Academy of Sciences of the United States of America*, *116*(18), 8657–8666.

Bell, M. L., Davis, D. L., & Fletcher, T. (2004). A retrospective assessment of mortality from the London smog episode of 1952: the role of influenza and pollution. *Environmental Health Perspectives*, *112*(1), 6–8.

Chen, D., Liu, Z., Ban, J., Zhao, P., & Chen, M. (2019a). Retrospective analysis of 2015–2017 wintertime PM2.5 in China: response to emission regulations and the role of meteorology. *Atmospheric Chemistry and Physics*, *19*(11), 7409–7427.

Chen, Z., Zhuang, Y., Xie, X., Chen, D., Cheng, N., Yang, L., & Li, R. (2019b). Understanding long-term variations of meteorological influences on ground ozone concentrations in Beijing during 2006–2016. *Environmental Pollution*, *245*, 29–37.

Cheng, J., Su, J., Cui, T., Li, X., Dong, X., Sun, F., . . . He, K. (2019). Dominant role of emission reduction in PM2.5 air quality improvement in Beijing during 2013–2017: A model-based decomposition analysis. *Atmospheric Chemistry and Physics*, *19*(9), 6125–6146.

Cheng, Y., Zheng, G., Wei, C., Mu, Q., Zheng, B., Wang, Z., . . . Su, H. (2016). Reactive nitrogen chemistry in aerosol water as a source of sulfate during haze events in China. *Science Advances*, *2*(12), e1601530.

Chu, B., Kerminen, V. M., Bianchi, F., Yan, C., Petäjä, T., & Kulmala, M. (2019). Atmospheric new particle formation in China. *Atmospheric Chemistry and Physics*, *19*(1), 115–138.

Dal Maso, M., Kulmala, M., Riipinen, I., Wagner, R., Hussein, T., Aalto, P. P., & Lehtinen, K. E. J. (2005). Formation and growth of fresh atmospheric aerosols: eight years of aerosol size distribution data from SMEAR II, Hyytiala, Finland. *Boreal Environment Research*, *10*(5), 323–336.

Davis, D. L., Bell, M. L., & Fletcher, T. (2002). A look back at the London smog of 1952 and the half century since. *Environmental Health Perspectives*, *110*(12), A734–A735.

Ding, A., Nie, W., Huang, X., Chi, X., Sun, J., Kerminen, V.-M., … Fu, C. (2016a). Long-term observation of air pollution-weather/climate interactions at the SORPES station: a review and outlook. *Frontiers of Environmental Science & Engineering*, *10*(5), 15.

Ding, A. J., Huang, X., Nie, W., Sun, J. N., Kerminen, V.-M., Petäjä, T., … Fu, C. B. (2016b). Enhanced haze pollution by black carbon in megacities in China. *Geophysical Research Letters*, *43*(6), 2873–2879.

Fröhlich, R., Cubison, M. J., Slowik, J. G., Bukowiecki, N., Prévôt, A. S. H., Baltensperger, U., … Jayne, J. T. (2013). The ToF-ACSM: a portable aerosol chemical speciation monitor with TOFMS detection. *Atmospheric Measurement Techniques*, *6*(11), 3225–3241.

Fu, G. Q., Xu, W. Y., Yang, R. F., Li, J. B., & Zhao, C. S. (2014). The distribution and trends of fog and haze in the North China plain over the past 30 years. *Atmospheric Chemistry and Physics*, *14*(21), 11949–11958.

Gao, W., Tan, G., Hong, Y., Li, M., Nian, H., Guo, C., … Zhou, Z. (2013). Development of portable single photon ionization time-of-flight mass spectrometer combined with membrane inlet. *International Journal of Mass Spectrometry*, *334*, 8–12.

Guo, S., Hu, M., Peng, J., Wu, Z., Zamora, M. L., Shang, D., … Zhang, R. (2020). Remarkable nucleation and growth of ultrafine particles from vehicular exhaust. *Proceedings of the National Academy of Sciences S of the United States of America*, *117*(7), 3427–3432.

Guo, S., Hu, M., Zamora, M. L., Peng, J., Shang, D., Zheng, J., … Zhang, R. (2014). Elucidating severe urban haze formation in China. *Proceedings of the National Academy of Sciences of the United States of America*, *111*(49), 17373–17378.

Hallquist, M., Munthe, J., Hu, M., Wang, T., Chan, C. K., Gao, J., … Thynell, M. (2016). Photochemical smog in China: scientific challenges and implications for air-quality policies. *National Science Review*, *3*(4), 401–403.

Hari, P., Petäjä, T., Bäck, J., Kerminen, V. M., Lappalainen, H. K., Vihma, T., … Kulmala, M. (2016). Conceptual design of a measurement network of the global change. *Atmospheric Chemistry and Physics*, *16*(2), 1017–1028.

He, H., Wang, Y., Ma, Q., Ma, J., Chu, B., Ji, D., … Hao, J. (2014). Mineral dust and NOx promote the conversion of SO_2 to sulfate in heavy pollution days. *Scientific Report*, *4*. doi:10.1038/srep04172

He, P. Z., Alexander, B., Geng, L., Chi, X. Y., Fan, S. D., Zhan, H. C., … Xie, Z. Q. (2018). Isotopic constraints on heterogeneous sulfate production in Beijing haze. *Atmospheric Chemistry and Physics*, *18*(8), 5515–5528.

Hidy, G. M. (2018). An historical experiment: Los Angeles smog evolution observed by blimp. *Journal of the Air & Waste Management Association*, *68*(7), 643–655.

Hu, B., Wang, Y., & Liu, G. (2007). Ultraviolet radiation spatio-temporal characteristics derived from the ground-based measurements taken in China. *Atmospheric Environment*, *41*(27), 5707–5718.

Huang, L., Zhao, Y., Li, H., & Chen, Z. (2015). Kinetics of heterogeneous reaction of sulfur dioxide on authentic mineral dust: effects of relative humidity and hydrogen peroxide. *Environmental Science & Technology*, *49*(18), 10797–10805.

Huang, R.-J., Zhang, Y., Bozzetti, C., Ho, K.-F., Cao, -J.-J., Han, Y., … Prevot, A. S. H. (2014). High secondary aerosol contribution to particulate pollution during haze events in China. *Nature*, *514*(7521), 218–222.

Jiang, J., Chen, M., Kuang, C., Attoui, M., & McMurry, P. H. (2011). Electrical mobility spectrometer using a iethylene glycol condensation particle counter for measurement of aerosol size distributions down to 1 nm. *Aerosol Science and Technology*, *45*, 510–521.

Jokinen, T., Sipilä, M., Junninen, H., Ehn, M., Lönn, G., Hakala, J., … Worsnop, D. R. (2012). Atmospheric sulphuric acid and neutral cluster measurements using CI-APi-TOF. *Atmospheric Chemistry and Physics*, *12*(9), 4117–4125.

Kerminen, V.-M., Chen, X., Vakkari, V., Petäjä, T., Kulmala, M., & Bianchi, F. (2018). Atmospheric new particle formation and growth: Review of field observations. *Environmental Research Letters*, *13*(10), 103003.

Krechmer, J., Lopez-Hilfiker, F., Koss, A., Hutterli, M., Stoermer, C., Deming, B., … de Gouw, J. (2018). Evaluation of a new reagent-ion source and focusing ion–molecule reactor for use in proton-transfer-reaction mass spectrometry. *Analytical Chemistry*, *90*(20), 12011–12018.

Kulmala, M. (2015). China's choking cocktail. *Nature*, *526*(7574), 497–499.

Kulmala, M. (2018). Build a global Earth observatory. *Nature*, *553*, 21–23.

Kulmala, M., Kerminen, V. M., Petaja, T., Ding, A. J., & Wang, L. (2017). Atmospheric gas-to-particle conversion: why NPF events are observed in megacities? *Faraday Discussions*, *200*(0), 271–288.

Kürten, A., Jokinen, T., Simon, M., Sipilä, M., Sarnela, N., Junninen, H., … Curtius, J. (2014). Neutral molecular cluster formation of sulfuric acid–dimethylamine observed in real time under atmospheric conditions. *Proceedings of the National Academy of Sciences of the United States of America*, *111*(42), 15019–15024.

Larssen, T., Lydersen, E., Tang, D., He, Y., Gao, J., Liu, H., … Luo, J. (2006). Acid rain in China. *Environmental Science & Technology*, *40*(2), 418–425.

Larssen, T., Seip, H. M., Semb, A., Mulder, J., Muniz, I. P., Vogt, R. D., … Eilertsen, O. (1999). Acid deposition and its effects in China: an overview. *Environmental Science & Policy*, *2*(1), 9–24.

Laughner, J. L., & Cohen, R. C. (2019). Direct observation of changing NOx lifetime in North American cities. *Science*, *366*(6466), 723–727.

Lelieveld, J., Evans, J. S., Fnais, M., Giannadaki, D., & Pozzer, A. (2015). The contribution of outdoor air pollution sources to premature mortality on a global scale. *Nature*, *525*(7569), 367–370.

Li, J., Lu, K., Lv, W., Li, J., Zhong, L., Ou, Y., … Zhang, Y. (2014). Fast increasing of surface ozone concentrations in Pearl river delta characterized by a regional air quality monitoring network during 2006–2011. *Journal of Environmental Sciences*, *26*(1), 23–36.

Liu, T., Gong, S., He, J., Yu, M., Wang, Q., Li, H., … Zhao, Q. (2017). Attributions of meteorological and emission factors to the 2015 winter severe haze pollution episodes in China's Jing-Jin-Ji area. *Atmospheric Chemistry and Physics*, *17*(4), 2971–2980.

Lopez-Hilfiker, F. D., Mohr, C., Ehn, M., Rubach, F., Kleist, E., Wildt, J., … Thornton, J. A. (2014). A novel method for online analysis of gas and particle composition: description and evaluation of a Filter Inlet for gases and AEROsols (FIGAERO). *Atmospheric Measurement Techniques*, *7*(4), 983–1001.

Ma, J. Z., Xu, X. B., Zhao, C. S., & Yan, P. (2012). A review of atmospheric chemistry research in China: photochemical smog, haze pollution, and gas-aerosol interactions. *Advances in Atmospheric Sciences*, *29*(5), 1006–1026.

Ma, Z., Hu, X., Sayer, A. M., Levy, R., Zhang, Q., Xue, Y., … Liu, Y. (2016). Satellite-based spatiotemporal trends in PM2.5 concentrations: China, 2004–2013. *Environmental Health Perspectives*, *124*(2), 184–192.

Manninen, H. E., Mirme, S., Mirme, A., Petäjä, T., & Kulmala, M. (2016). How to reliably detect molecular clusters and nucleation mode particles with neutral cluster and air ion spectrometer (NAIS). *Atmospheric Measurement Techniques*, *9*(8), 3577–3605.

Mirme, S., & Mirme, A. (2013). The mathematical principles and design of the NAIS – A spectrometer for the measurement of cluster ion and nanometer aerosol size distributions. *Atmospheric Measurement Techniques*, *6*(4), 1061–1071.

Petäjä, T., Duplissy, E.-M., Tabakova, K., Schmale, J., Altstädter, B., Ancellet, G., … Lappalainen, H. K. (2020). Integrative and comprehensive understanding on polar environments (iCUPE): the concept and initial results. *Atmospheric Chemistry and Physics*, *20*, 8551–8592.

Petäjä, T., Järvi, L., Kerminen, V.-M., Ding, A., Sun, J., Nie, W., … Kulmala, M. (2016). Enhanced air pollution via aerosol-boundary layer feedback in China. *Scientific Reports*, *6*, 18998.

Quan, J., Dou, Y., Zhao, X., Liu, Q., Sun, Z., Pan, Y., … Liu, Y. (2020). Regional atmospheric pollutant transport mechanisms over the North China plain driven by topography and planetary boundary layer processes. *Atmospheric Environment*, *221*, 117098.

Shao, M., Tang, X., Zhang, Y., & Li, W. (2006). City clusters in China: air and surface water pollution. *Frontiers in Ecology and the Environment*, *4*(7), 353–361.

Smith, J. N., Moore, K. F., McMurry, P. H., & Eisele, F. L. (2004). Atmospheric measurements of sub-20 nm diameter particle chemical composition by thermal desorption chemical ionization mass spectrometry. *Aerosol Science and Technology*, *38*(2), 100–110.

Sun, J., Zhang, Q., Manjula, C., Zhang, Y., Ng, N. L., Sun, Y., … Worsnop, D. R. (2010). Highly time- and size-resolved characterization of submicron aerosol particles in Beijing using an Aerodyne aerosol mass spectrometer. *Atmospheric Environment*, *44*, 131–140.

Sun, P., Nie, W., Chi, X., Xie, Y., Huang, X., Xu, Z., … Ding, A. (2018). Two years of online measurement of fine particulate nitrate in the western Yangtze river delta: influences of thermodynamics and N$_2$O$_5$ hydrolysis. *Atmospheric Chemistry and Physics*, *18*(23), 17177–17190.

Sun, Y. L., Wang, Z. F., Du, W., Zhang, Q., Wang, Q. Q., Fu, P. Q., … Worsnop, D. R. (2015). Long-term real-time measurements of aerosol particle composition in Beijing, China: seasonal variations, meteorological effects, and source analysis. *Atmospheric Chemistry and Physics*, *15*(17), 10149–10165.

Tan, G.-B., Gao, W., Huang, Z.-X., Hong, Y., Fu, Z., Dong, J.-G., … Zhou, Z. (2011). Vacuum ultraviolet single-photon ionization time-of-flight mass spectrometer. *Chinese Journal of Analytical Chemistry*, *39*(10), 1470–1475.

Tang, G., Li, X., Wang, Y., Xin, J., & Ren, X. (2009). Surface ozone trend details and interpretations in Beijing, 2001–2006. *Atmospheric Chemistry and Physics*, *9*(22), 8813–8823.

Tang, L., Qu, J., Mi, Z., Bo, X., Chang, X., Anadon, L. D., … Zhao, X. (2019). Substantial emission reductions from Chinese power plants after the introduction of ultra-low emissions standards. *Nature Energy*, *4*, 929–938.

Tang, X., Li, J., & Dong, Z. (1989). Photochemical pollution in Lanzhou, China-a case study. *Journal of Environmental Sciences (China)*, *1*, 31–38.

Tian, B., Jing, S., Ma, Y., Tian, W., Gu, X., Zheng, J., … Xu, Y. (1980). Study on photochemical smog pollution in at Xigu distrcit in Lanzhou. *Environmental Science (In Chinese)*, *1*(5), 24–30.

Tong, S., Hou, S., Zhang, Y., Chu, B., Liu, Y., He, H., … Ge, M. (2015). Comparisons of measured nitrous acid (HONO) concentrations in a pollution period at urban and suburban Beijing, in autumn of 2014. *Science China. Chemistry*, *58*(9), 1393–1402.

Tong, S., Hou, S., Zhang, Y., Chu, B., Liu, Y., He, H., … Ge, M. (2016). Exploring the nitrous acid (HONO) formation mechanism in winter Beijing: Direct emissions and heterogeneous production in urban and suburban areas. *Faraday Discussions*, *189*, 213–230.

Vanhanen, J., Mikkilä, J., Lehtipalo, K., Sipilä, M., Manninen, H. E., Siivola, E., … Kulmala, M. (2011). Particle size magnifier for nano-CN detection. *Aerosol Science and Technology*, *45*(4), 533–542.

Wang, G., Zhang, R., Gomez, M. E., Yang, L., Zamora, M. L., Hu, M., … Molina, M. J. (2016). Persistent sulfate formation from London fog to Chinese haze. *Proceedings of the National Academy of Sciences of the United States of America*, *113*((48)), 13630–13635.

Wang, L. T., Wei, Z., Yang, J., Zhang, Y., Zhang, F. F., Su, J., … Zhang, Q. (2014). The 2013 severe haze over southern Hebei, China: model evaluation, source apportionment, and policy implications. *Atmospheric Chemistry and Physics*, *14*(6), 3151–3173.

Wang, T., & Kwok, J. Y. H. (2003). Measurement and analysis of a multiday photochemical smog episode in the Pearl river delta of China. *Journal of Applied Meteorology*, *42*(3), 404–416.

Wang, T., Xue, L., Brimblecombe, P., Lam, Y. F., Li, L., & Zhang, L. (2017a). Ozone pollution in China: a review of concentrations, meteorological influences, chemical precursors, and effects. *Science of the Total Environment*, *575*, 1582–1596.

Wang, Y., Yu, M., Wang, Y., Tang, G., Song, T., Zhou, P., … Petäjä, T. (2020). Rapid formation of intense haze episodes via aerosol–boundary layer feedback in Beijing. *Atmospheric Chemistry and Physics*, *20*(1), 45–53.

Wang, Y. S., Teter, J., & Sperling, D. (2011). China's soaring vehicle population: Even greater than forecasted? *Energy Policy*, *39*(6), 3296–3306.

Wang, Z., Wang, W., Tham, Y. J., Li, Q., Wang, H., Wen, L., . . . Wang, T. (2017b). Fast heterogeneous N2O5 uptake and ClNO2 production in power plant and industrial plumes observed in the nocturnal residual layer over the North China plain. *Atmospheric Chemistry and Physics*, *17*(20), 12361–12378.

Wen, L., Xue, L., Wang, X., Xu, C., Chen, T., Yang, L., . . . Wang, W. (2018). Summertime fine particulate nitrate pollution in the North China plain: increasing trends, formation mechanisms and implications for control policy. *Atmospheric Chemistry and Physics*, *18*(15), 11261–11275.

Xue, J., Yu, X., Yuan, Z., Griffith, S. M., Lau, A. K. H., Seinfeld, J. H., & Yu, J. Z. (2019). Efficient control of atmospheric sulfate production based on three formation regimes. *Nature Geoscience*, *12*(12), 977–982.

Yao, L., Garmash, O., Bianchi, F., Zheng, J., Yan, C., Kontkanen, J., . . . Wang, L. (2018). Atmospheric new particle formation from sulfuric acid and amines in a Chinese megacity. *Science*, *361*(6399), 278–281.

Yatavelli, R. L. N., Mohr, C., Stark, H., Day, D. A., Thompson, S. L., Lopez-Hilfiker, F. D., . . . Jimenez, J. L. (2015). Estimating the contribution of organic acids to northern hemispheric continental organic aerosol. *Geophysical Research Letters*, *42*(14), 6084–6090.

Yu, H., He, N., Wang, Q., Zhu, J., Gao, Y., Zhang, Y., . . . Yu, G. (2017a). Development of atmospheric acid deposition in China from the 1990s to the 2010s. *Environmental Pollution*, *231*, 182–190.

Yu, Q., Zhang, T., Ma, X. X., Kang, R. H., Mulder, J., Larssen, T., & Duan, L. (2017b). Monitoring effect of SO_2 emission abatement on recovery of acidified soil and streamwater in southwest China. *Environmental Science & Technology*, *51*(17), 9498–9506.

Zamora, M. L., Peng, J., Hu, M., Guo, S., Marrero-Ortiz, W., Shang, D., . . . Zhang, R. (2019). Wintertime aerosol properties in Beijing. *Atmospheric Chemistry and Physics*, *19*(22), 14329–14338.

Zhang, F., Wang, Y., Peng, J., Chen, L., Sun, Y., Duan, L., . . . Zhang, R. (2020). An unexpected catalyst dominates formation and radiative forcing of regional haze. *Proceedings of the National Academy of Sciences of the United States of America*, *117*(8), 3960–3966.

Zhang, J. F., & Samet, J. M. (2015). Chinese haze versus Western smog: Lessons learned. *Journal of Thoracic Disease*, *7*(1), 3–13.

Zhang, Q., Jiang, X., Tong, D., Davis, S. J., Zhao, H., Geng, G., . . . Guan, D. (2017). Transboundary health impacts of transported global air pollution and international trade. *Nature*, *543*(7647), 705–709.

Zhang, Q., Zheng, Y., Tong, D., Shao, M., Wang, S., Zhang, Y., . . . Hao, J. (2019). Drivers of improved $PM_{2.5}$ air quality in China from 2013 to 2017. *Proceedings of the National Academy of Sciences of the United States of America*, *116*(49), 24463–24469.

Zhang, R., Wang, G., Guo, S., Zamora, M. L., Ying, Q., Lin, Y., . . . Wang, Y. (2015). Formation of urban fine particulate matter. *Chemical Reviews*, *115*(10), 3803–3855.

Zhang, X. Y., Zhong, J. T., Wang, J. Z., Wang, Y. Q., & Liu, Y. J. (2018). The interdecadal worsening of weather conditions affecting aerosol pollution in the Beijing area in relation to climate warming. *Atmospheric Chemistry and Physics*, *18*(8), 5991–5999.

Zheng, G. J., Duan, F. K., Su, H., Ma, Y. L., Cheng, Y., Zheng, B., . . . He, K. B. (2015). Exploring the severe winter haze in Beijing: the impact of synoptic weather, regional transport and heterogeneous reactions. *Atmospheric Chemistry and Physics*, *15*(6), 2969–2983.

Zheng, X., Lu, Y., Yuan, J., Baninla, Y., Zhang, S., Stenseth, N. C., . . . Chen, D. (2020). Drivers of change in China's energy-related CO_2 emissions. *Proceedings of the National Academy of Sciences of the United States of America*, *117*(1), 29–36.

Zhong, J., Zhang, X., Dong, Y., Wang, Y., Liu, C., Wang, J., . . . Che, H. (2018). Feedback effects of boundary-layer meteorological factors on cumulative explosive growth of $PM_{2.5}$ during winter heavy pollution episodes in Beijing from 2013 to 2016. *Atmospheric Chemistry and Physics*, *18*(1), 247–258.

Zhu, W. H., Xu, X. D., Zheng, J., Yan, P., Wang, Y. J., & Cai, W. Y. (2018). The characteristics of abnormal wintertime pollution events in the Jing-Jin-Ji region and its relationships with meteorological factors. *Science of the Total Environment*, *626*, 887–898.